Suppression of Leakage Current in Wireless Charging Systems Using n-legged Inverters

1st Yusaku Takagi
Graduate School of Frontier Sciences
The University of Tokyo
Kashiwa, Chiba, Japan
Email: takagi.yusaku22@ae.k.u-tokyo.ac.jp

2nd Tatsuya Yanagi
Research and Development Center
ROHM Co., Ltd.
Kyoto, Kyoto, Japan
Email: tatsuya.yanagi@dsn.rohm.co.jp

3rd Hiroshi Fujimoto
Graduate School of Frontier Sciences
The University of Tokyo
Kashiwa, Chiba, Japan
Email: fujimoto@k.u-tokyo.ac.jp

***Abstract*—An n-legged inverter for driving n−1 transmitter coils has been proposed to reduce the implementation costs of wireless power transfer (WPT) systems for the dynamic charging of electric vehicles (EVs). However, leakage current flowing through uncoupled coils deteriorates system efficiency and causes leakage electromagnetic interference (EMI). Suppression of leakage current by switching of legs not directly used for wireless charging is preferable as it requires no additional components. However, turning the unused legs off can be insufficient, while switching them identically to adjacent legs causes large switching losses and is potentially counterproductive. A novel switching method of unused legs is proposed to greatly suppress leakage current with limited losses.**

***Index Terms*—n-legged Inverter, Wireless Charging, Leakage Current, Output Capacitance, Dead Time, Resonant Circuit**

I. Introduction

Limiting global warming to $1.5\,^{\circ}\mathrm{C}$ will avoid its worst outcomes, but will require immediate and deep emissions reductions of greenhouse gas (GHG) across all sectors [1]. The transport sector accounted for roughly $15\,\%$ of total GHG emissions in 2019, $70\,\%$ of which came from road transport, with light-duty vehicles for passenger transport representing the largest share. Electric vehicles (EVs) powered by low-emissions electricity offer the most considerable decarbonization potential for such vehicles, but the limited driving distance and long charging time limit their market appeal [2].

Dynamic wireless power transfer (DWPT) is gaining traction as a solution to both problems. Inductive DWPT systems wirelessly charge EVs while they are in motion by the magnetic coupling of coils. DWPT would remove limitations of EVs on driving distance, remove the need to recharge, and allow for a lighter battery, thereby reducing the driving resistance and hence, CO_2 emissions [3].

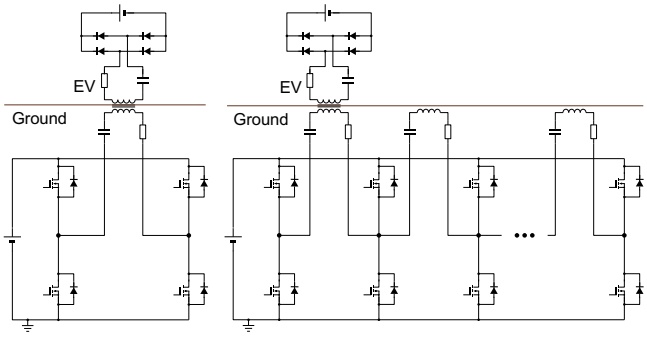

(a) Full-bridge inverter (b) n-legged inverter

Fig. 1. A full-bridge inverter and an n-legged inverter.

Implementing a DWPT system with a full-bridge inverter to drive each transmitter coil can be expensive, as the inverter is a sizable portion of the cost [4]. Various circuit and converter topologies have been proposed [5]–[22] to reduce the inverter cost, such as a common full-bridge inverter driving multiple transmitter coils connected in parallel [6]–[10]. However, while this topology would reduce the number of switches for n transmitter coils to 4+2n switches from the 4n switches required for individual full-bridge inverters, it would increase the maximum current stress on the switches by a factor of n [16].

n-legged inverters driving n−1 transmitter coils can reduce the number of switches for n transmitter coils to 2+2n without increasing the maximum current or voltage stress on the switches [19]–[22]. Fig. 1 shows a full-bridge inverter with 1 transmitter coil and an n-legged inverter with n−1 transmitter coils. n-legged inverters consist of n half-bridge inverters, called legs, each with a high-side switch and a low-side switch, each called arms.

In an n-legged inverter, where the n−1 transmitter coils are connected electrically, leakage current has been known to flow through uncoupled coils when at least one of the coils is wirelessly charging a receiver unit [20], [21]. Leakage current can cause copper losses and electromagnetic interference (EMI) [23] and therefore require suppression. In previous research, the unused legs, *e.g.* the third leg from the left in Fig. 1(b), are either switched off or switched identically to their adjacent leg, *e.g.* the second leg from the left. However, these methods are insufficient with high power output or a large number of legs.

This article aims to eliminate leakage current without the use of additional components. A novel switching method for unused legs is proposed, which significantly reduces leakage current. In the following sections, the circuit operation regarding the uncoupled coils and the unused legs is explained in detail. Section II provides an explanation of the principle of leakage current in conventional methods using a 3-legged

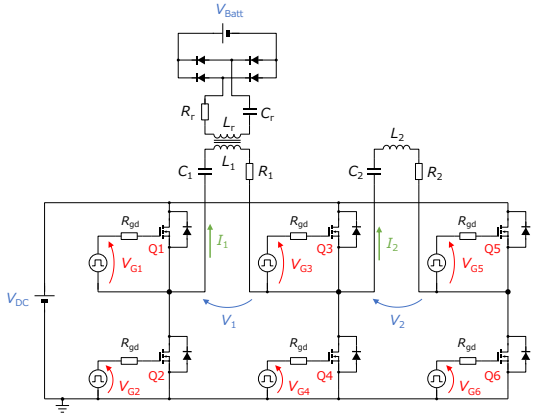

Fig. 2. A wireless power transfer system with a 3-legged inverter. Only one of the two transmitter coils is connected to a receiver coil.

inverter system as an example. Section III describes the proposed switching method. Section IV presents and compares experimental results with simulation results. Finally, section V concludes the article.

II. Conventional Methods

Fig. 2 shows a 3-legged inverter WPT system driving 2 transmitter coils, one of which is coupled with a receiver coil. In such systems, the inductance and the capacitance are tuned so that they resonate at a certain frequency f, which for this system is 85 kHz. V_{M1}, V_{M2}, and V_{M3} are the leg-ground voltage of each leg, and $V_1 = V_{M1} - V_{M2}$ is the load voltage while $V_2 = V_{M2} - V_{M3}$ is the voltage applied to the uncoupled load. I_1 and I_2 each represent the current flowing through coil 1, the coupled coil, and coil 2, the uncoupled coil. The parameters of this system, measured prior to the experiment and used in the simulation, are shown in Table I. The parameters were measured using the Hioki IM3533 model LCR Meter. 4 S4103 SiC MOSFET SPICE models (ROHM Co., Ltd.) were connected in parallel for each arm, and STTH200L06TV1 SPICE models (STMicroelectronics) were used for the rectifier.

In the 3-legged inverter shown in Fig. 2, Q1–Q4 operate like a full-bridge inverter while Q5 and Q6 have no predetermined behavior. In [20] and [21], Q5 and Q6 are either turned off or switched identically to Q3 and Q4. The corresponding gate driver outputs and the ideal voltages they apply are shown in Fig. 3. Turning the switches off leaves V_2 uncontrolled while switching them identically to Q3 and Q4 ideally keeps V_2 at 0 V, suppressing leakage current I_2. However, the experimental results from previous research suggest that these methods are insufficient in preventing leakage current from flowing through uncoupled coils.

Fig. 4 shows the LTspice-simulated results of load voltage V_1 and leakage current I_2. The first green wave shows I_2 when Q5 and Q6 are turned off and the second green wave shows I_2 when Q5 and Q6 switch identically to Q3 and Q4. The results suggest that with higher power output,leakage current

TABLE I
Circuit Parameters.

Parameter	Symbol	Value
DC Voltage	V_{DC}	120 V
Transmitter resistance	R_1,R_2	264 mΩ, 392 mΩ
Transmitter coil self-inductance	L_1,L_2	247.5 µH, 244.6 µH
Transmitter capacitance	C_1,C_2	14.2 nF, 14.9 nF
Receiver resistance	R_r	77.7 mΩ
Receiver coil self-inductance	L_r	99.4 µH
Receiver capacitance	C_r	35 nF
Mutual inductance	M_1	21.1 µH
Battery Voltage	V_{Batt}	120 V
Resonant frequency	$f(=\omega/2\pi)$	85 kHz
Gate drive resistance	R_{gd}	4.7 Ω
Gate ON Voltage	V_{ON}	20.5 V
Gate OFF Voltage	V_{OFF}	−4 V
Gate Driver Voltage	$V_{Gi}(1 \le i \le 6)$	
Dead time	T_{dt}	350 ns
Output Capacitance	C_{OSS}	852 pF
Length of full pulse	T_{ON}	$\frac{1}{2}\frac{1}{f} - T_{dt}$
Length of proposed pulse	ΔT_S	

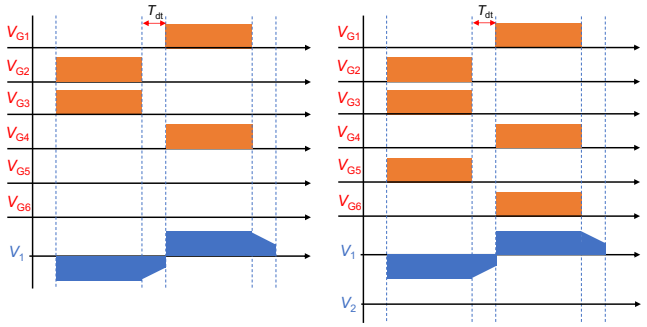

(a) Off (b) Identical

Fig. 3. Gate driver outputs for Q1–Q6 and ideal voltage waveforms for V_1 and V_2. When Q5 and Q6 are turned off, uncoupled load voltage V_2 is not controlled.

I_2 may increase enough to cause large copper loss and EMI. We further examine the principle behind this leakage current.

A. No Switching

When a switch is turned off, it can be regarded as its output capacitance C_{OSS}. Therefore, because Q5 and Q6 are turned off, they can be regarded as capacitors 5 and 6. V_{M3} is decided by the voltages of capacitors 5 and 6. Therefore, if we assume I_2 flows because of the difference in potential between V_{M2} and V_{M3}, then I_2 must charge or discharge capacitors 5 and 6, as V_{M2} is decided by the switching of Q3 and Q4 and therefore any effect of I_2 on V_{M2} is negligible.

Fig. 5 shows leakage current I_2 with leg-ground voltages V_{M2} and V_{M3}, when Q5 and Q6 are turned off. The waveforms are divided into 2 flows to explain the corresponding current routes, shown in Figs. 6(a)–6(b). Q5 and Q6 are replaced with capacitors 5 and 6 for clarity. In flow 1, I_2 charges capacitor 6 and discharges capacitor 5. This corresponds to V_{M3} increasing during flow 1 in Fig. 5. In flow 2, the capacitors are fully charged or discharged and I_2 flows through the body diode of

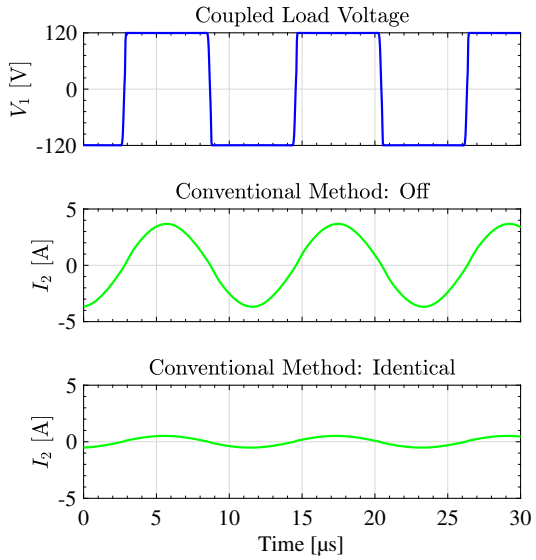

Fig. 4. Simulation results for leakage current I_2 and load voltage V_1. Each waveform corresponds to when Q5 and Q6 are off or when they switch identically to Q3 and Q4.

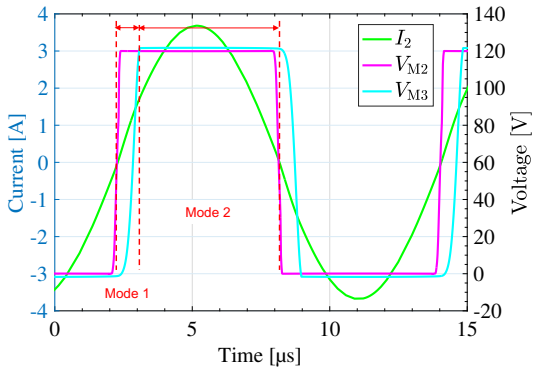

Fig. 5. Simulated waveforms for I_2, V_{M2}, and V_{M3}. 2 current flows are shown for when I_2 is positive. The same goes for when I_2 is negative.

Q5. This corresponds to V_{M3} being slightly higher than V_{DC} in Fig. 5 due to the voltage drop from the body diode. The same principle can be applied when Q4 is turned on. I_2, in this case, can therefore be understood to flow because of the difference in potential between V_{M2} and V_{M3}.

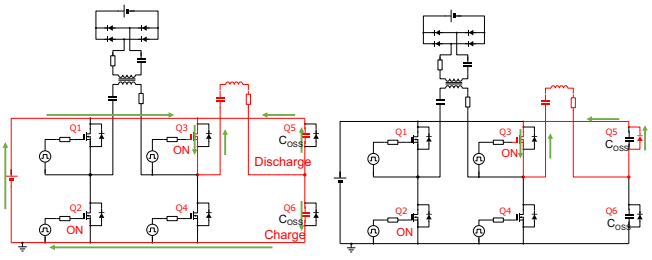

(a) Flow 1 (b) Flow 2

Fig. 6. Current flows for when Q5 and Q6 are off and I_2 is positive.

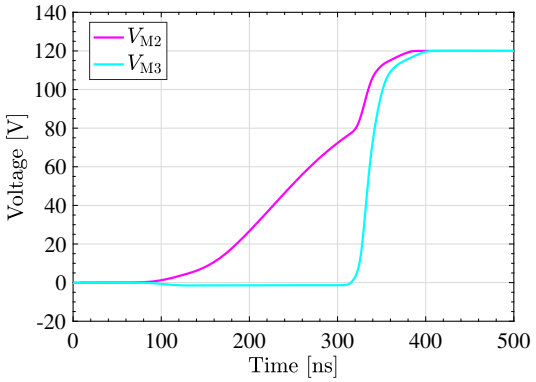

Fig. 7. V_{M2} and V_{M3} during dead time.

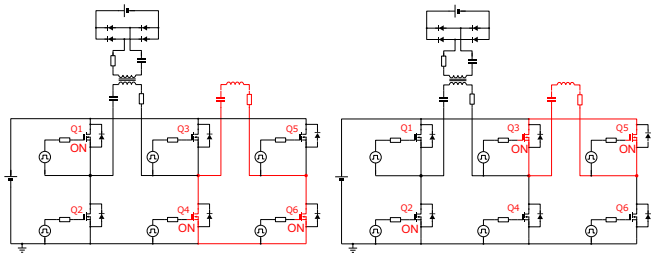

(a) Route 1 (b) Route 2

Fig. 8. RLC resonant loops that form when Q5 and Q6 switch at the same pattern as Q3 and Q4.

B. Identical Switching

The ideal V_2 shown in Fig. 3(b) is complicated by the dead time between switch turn off and turn on, when all switches are turned off. Dead times are put in place to prevent the high-side switch and the low-side switch from turning on at the same time, for device protection. During dead time, V_{M2} and V_{M3} are uncontrolled and a difference in potential can occur. Fig. 7 shows V_{M2} and V_{M3} during the dead time from Q4 turn-off to Q3 turn-on. V_{M2} increases because I_1 charges the output capacitance of Q4. V_{M3} does not increase because I_2 is significantly smaller than I_1 and because the phase of I_2 is such that it flows through the body diode of Q6 during dead time.

The V_2 applied during dead time causes I_2 to flow partly through the RLC resonant circuits shown in Fig. 8, which occur when either Q3 and Q5 or Q4 and Q6 are turned on at the same time. Because L_2 and C_2 are tuned to resonate at whatever frequency the circuit operates in, and R_2 is engineered to be as small as possible, the impedances of these loops are very small. The relationship between I_2 and dead time is shown in Fig. 9, which shows the simulated RMS values of the fundamental component of I_2 with respect to dead time. I_2 increases as dead time becomes longer because V_2 increases, as explained above. This relationship holds as long as the phase of I_1 is such that V_{M2} increases during dead time.

This principle suggests that shortening the dead time or

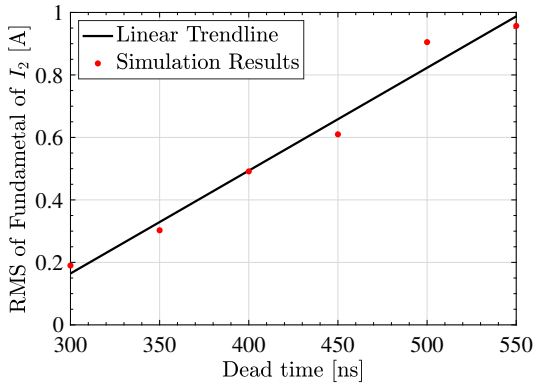

Fig. 9. RMS Values of fundamental components of I_2 for dead times ranging from 300 ns to 550 ns. I_2 increases as dead time increases.

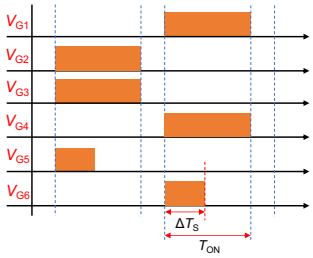

Fig. 10. Proposed gate driver outputs. Q5 and Q6 send pulses.

causing I_1 to have a large enough leading power factor to keep V_{M2} from increasing would suppress I_2. Although these would work, the former is not recommended as the dead time is necessary for device protection, and the latter would cause a hard turn-on, which would increase switching loss and worsen inverter efficiency.

III. Proposed Short Pulse Switching

Fig. 10 shows the gate driver output of the proposed short-pulse switching method. V_{G5} and V_{G6} each rises at the same time as V_{G3} and V_{G4}, and then falls after ΔT_S seconds. The proposed method of turning Q5 or Q6 on shortly and then turning them off is intended to remove the causes of I_2 described in the preceding section. By turning Q5 or Q6 on shortly, it allows the current required for the charging of the output capacitance of the opposing switch to flow through the turned-on switch and not coil 2. By then turning them off, it blocks the RLC resonant circuit shown in Fig. 8 from forming. Fig. 11 shows the simulated waveform for a pulse with $\frac{\Delta T_S}{T_{ON}} = 0.15$.

The RMS values of the three methods, as well as the copper loss and the DC/AC efficiency, are shown in Table II. The results show that the proposed method has the smallest value of I_2 and a significantly smaller copper loss than the conventional methods. The DC/AC efficiency is also the best with the proposed method.

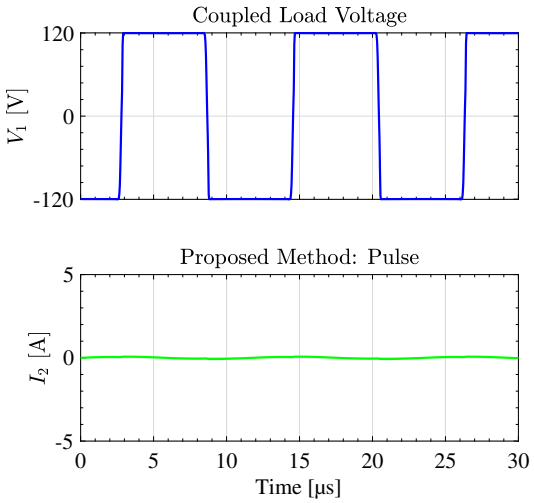

Fig. 11. Simulation results for leakage current I_2 with the proposed short-pulse method, with a $\frac{\Delta T_S}{T_{ON}} = 0.15$.

TABLE II
Simulation Results.

Switching	RMS of I_2	Copper Loss	DC/AC Efficiency
Off	2.67 A	3.26 W	99.0 %
Full Pulse	388 mA	64.1 mW	99.1 %
Pulse (proposed)	46 mA	0.55 mW	99.2 %

IV. Experiment

The effectiveness of the proposed method was confirmed by experiments. The circuit diagram of the experiment is shown in Fig. 2, the parameters are shown in Table I, and the measurement equipment and power supply are shown in Table III. The transmitter coil and receiver coil [24] are shown in Fig. 12, and the inverter is shown in Fig. 13. Four parallelly connected S4103 SiC MOSFETs made by ROHM Co., Ltd. are used for each arm. STTH200L06TV1 rectifiers made by STMicroelectronics were used for the receiver unit. $\frac{\Delta T_S}{T_{ON}} = 0.15$ was chosen for the proposed switching.

The experiment results are shown in Fig. 14. The blue waveform shows the load voltage V_1 and the following green waveforms each correspond to when Q5 and Q6 are off, switched identically to Q3 and Q4, and switched with the proposed short pulses. The RMS values of I_2 are shown in Table IV. The proposed short pulse switching achieves the smallest I_2.

TABLE III
Equipment.

Equipment	Model
DC Power Supply	TAKASAGO ZX-S-1600MA
Control System	PE-Expert4 MWPE4-RACK12 IPFPGA24
DC Battery	headspring biATLAS-D
Oscilloscope	Tektronix MDO34
Current Probe	Tektronix TCP0020, TCP0150
Differential Probe	Tektronix THDP0200

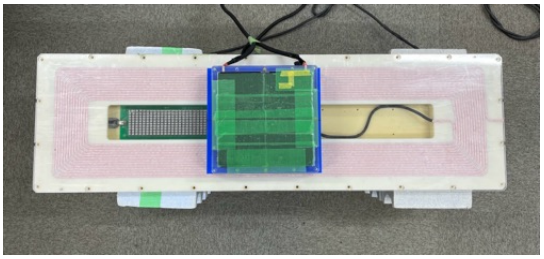

Fig. 12. Transmitter coil and Receiver coil used in the experiment.

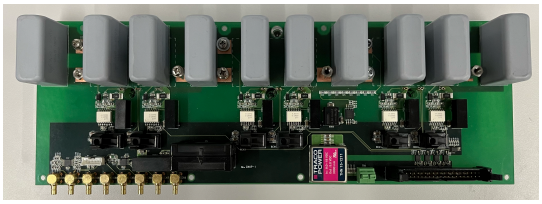

Fig. 13. 3-legged inverter used in the experiment.

The RMS of I_2 is a function of the ratio between ΔT_S and T_ON, $\frac{\Delta T_\mathrm{S}}{T_\mathrm{ON}}$. Fig. 15 shows the experiment results of the RMS values of I_2 with respect to the $\frac{\Delta T_\mathrm{S}}{T_\mathrm{ON}}$ of the pulse, for $\frac{\Delta T_\mathrm{S}}{T_\mathrm{ON}} = 0$ to $\frac{\Delta T_\mathrm{S}}{T_\mathrm{ON}} = 0.2$. $\frac{\Delta T_\mathrm{S}}{T_\mathrm{ON}} = 0$ corresponds to when Q5 and Q6 are turned off. The results show that I_2 has a minimum value at $\frac{\Delta T_\mathrm{S}}{T_\mathrm{ON}} = 0.03$. The $\frac{\Delta T_\mathrm{S}}{T_\mathrm{ON}}$ which gives the smallest I_2 depends on the C_OSS of the switches, as the principle explained in Section II-A shows.

V. Conclusion

In this article, a novel switching method for unused legs in n-legged inverters is proposed to suppress the leakage current that flows through uncoupled coils. The conventional methods of turning off the switch and switching identically to the adjacent leg are described, and a method to suppress the leakage current by applying a short charging pulse is proposed. The validity of the proposed method is confirmed through simulation and experiments.

Further research should focus on optimizing the length of the pulse and developing control methods to constantly minimize leakage current. The validity of the proposed method in inverters with four or more legs also needs to be explored. Additionally, increasing the power and reducing switching losses remain a challenge. It is desirable to minimize accompanying switching losses to be lower than the reduction in copper losses achieved through the suppression of leakage current.

TABLE IV
Experiment Results.

Switching	RMS of I_2
Off	642.3 mA
Identical	1.075 A
Pulse (proposed)	62.4 mA

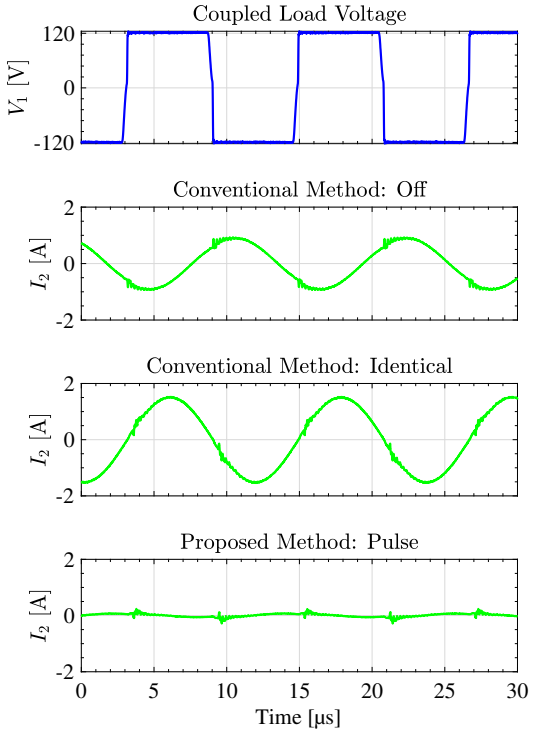

Fig. 14. Experiment results of I_2. I_2 is the smallest with a short pulse.

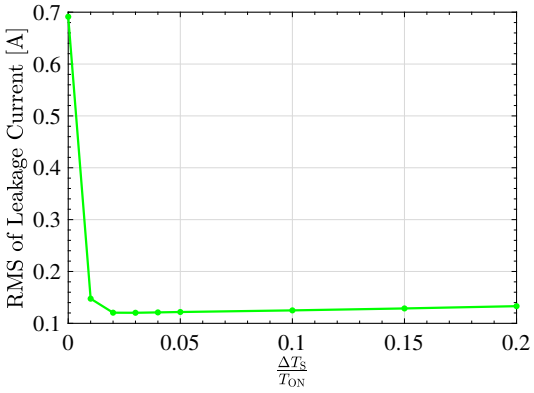

Fig. 15. The RMS of I_2 with respect to the $\frac{\Delta T_\mathrm{S}}{T_\mathrm{ON}}$ of charging pulse.

Acknowledgment

This work was partly supported by JST-Mirai Program Grant Number JPMJMI21E2 and the New Energy and Industrial Technology Development Organization (NEDO) Project Number JPNP21005, Japan.

References

[1] P. R. Shukla, J. Skea, R. Slade, A. Al Khourdajie, R. van Diemen, D. McCollum, M. Pathak, S. Some, P. Vyas, R. Fradera, M. Belkacemi, A. Hasija, G. Lisboa, S. Luz, J. Malley, (eds.), "IPCC, 2022: Climate Change 2022: Mitigation of Climate Change. Contribution of Working Group III to the Sixth Assessment Report of the Intergovernmental Panel on Climate Change", Cambridge University Press, Cambridge, UK and New York, NY, USA, 2022.

[2] G. A. Covic and J. T. Boys, "Inductive Power Transfer," *Proceedings of the IEEE*, vol. 101, no. 6, pp. 1276-1289, Jun. 2013.

[3] O. Shimizu, S. Nagai, T. Fujita, and H. Fujimoto, "Potential for CO2 Reduction by Dynamic Wireless Power Transfer for Passenger Vehicles in Japan," Energies, vol. 13, no. 13, p. 3342, Jun. 2020.

[4] V. Cirimele, M. Diana, F. Freschi, and M. Mitolo, "Inductive Power Transfer for Automotive Applications: State-of-the-Art and Future Trends," *IEEE Transactions on Industry Applications*, vol. 54, no. 5, pp. 4069-4079, Sept.-Oct. 2018.

[5] S. Choi, J. Huh, W. Y. Lee, S. W. Lee, and C. T. Rim, "New Cross-Segmented Power Supply Rails for Roadway-Powered Electric Vehicles," *IEEE Transactions on Power Electronics*, vol. 28, no. 12, pp. 5832-5841, Dec. 2013.

[6] N. Madzharov and V. Petkov, "Innovative solution of static and dynamic contactless charging station for electrical vehicles," *PCIM Europe 2016; International Exhibition and Conference for Power Electronics, Intelligent Motion, Renewable Energy and Energy Management*, Nuremberg, Germany, pp. 1-8., May 2016.

[7] S. Zhou and C. Chris Mi, "Multi-Paralleled LCC Reactive Power Compensation Networks and Their Tuning Method for Electric Vehicle Dynamic Wireless Charging," *IEEE Transactions on Industrial Electronics*, vol. 63, no. 10, pp. 6546-6556, Oct. 2016.

[8] A. C. Bagchi, A. Kamineni, R. A. Zane, and R. Carlson, "Review and Comparative Analysis of Topologies and Control Methods in Dynamic Wireless Charging of Electric Vehicles," *IEEE Journal of Emerging and Selected Topics in Power Electronics*, vol. 9, no. 4, pp. 4947-4962, Aug. 2021.

[9] Y. Li, J. Hu, T. Lin, X. Li, F. Chen, Z. He, and R. Mai, "A new coil structure and its optimization design with constant output voltage and constant output current for Electric Vehicle Dynamic Wireless Charging," *IEEE Transactions on Industrial Informatics*, vol. 15, no. 9, pp. 5244–5256, Sept. 2019.

[10] X. Li, J. Hu, H. Wang, X. Dai, and Y. Sun, "A New Coupling Structure and Position Detection Method for Segmented Control Dynamic Wireless Power Transfer Systems," *IEEE Transactions on Power Electronics*, vol. 35, no. 7, pp. 6741-6745, July 2020.

[11] H. Sumiya, E. Takahashi, N. Yamaguchi, K. Tani, S. Nagai, T. Fujita, and H. Fujimoto, "Coil scaling law of wireless power transfer systems for electromagnetic field leakage evaluation for electric vehicles", *IEEJ Journal of Industry Applications*, vol. 10, no. 5, pp. 575–576, Nov. 2021.

[12] C. Cai, M. Saeedifard, J. Wang, P. Zhang, J. Zhao, and Y. Hong, "A Cost-Effective Segmented Dynamic Wireless Charging System With Stable Efficiency and Output Power," *IEEE Transactions on Power Electronics*, vol. 37, no. 7, pp. 8682-8700, July 2022.

[13] J. Rahulkumar., R. Narayanamoorthi., P. Vishnuram, M. Bajaj, V. Blazek, L. Prokop, and S. Misak, "An empirical survey on wireless inductive power pad and resonant magnetic field coupling for in-motion EV charging system," *IEEE Access*, vol. 11, pp. 4660–4693, 2023.

[14] I. Karakitsios, E. Karfopoulos, N. Madjarov, A. Bustillo, M. Ponsar, D. Del Pozo, and L. Marengo, "An integrated approach for dynamic charging of electric vehicles by wireless power transfer - lessons learned from real-life implementation," *SAE International Journal of Alternative Powertrains*, vol. 6, no. 1, pp. 15–24, May 2017.

[15] Y. Tian, J. Tian, D. Li, and S. Zhou, "A Multiple Legs Inverter with Real Time–Reflected Load Detection Used in the Dynamic Wireless Charging System of Electric Vehicles," *Energies*, vol. 11, no. 5, p. 1275, May 2018.

[16] V. Z. Barsari, D. J. Thrimawithana, and G. A. Covic, "An Inductive Coupler Array for In-Motion Wireless Charging of Electric Vehicles," *IEEE Transactions on Power Electronics*, vol. 36, no. 9, pp. 9854-9863, Sept. 2021.

[17] H. Qiu, T. Sakurai, and M. Takamiya, "A 6.78-MHz Multiple-Transmitter Wireless Power Transfer System With Efficiency Maximization by Adaptive Magnetic Field Adder IC," *IEEE Journal of Solid-State Circuits*, vol. 57, no. 8, pp. 2390-2403, Aug. 2022.

[18] M. Aganti, K. B, L. R, and C. Bharatiraja, "Half bridge based multi leg converter for dynamic EV charging system," *2023 IEEE IAS Global Conference on Renewable Energy and Hydrogen Technologies (GlobConHT)*, 2023.

[19] J. Shin, S. Shin, Y. Kim, S. Ahn, S. Lee, G. Jung, S.-J. Jeon, and D.-H. Cho, "Design and implementation of shaped magnetic-resonance-based wireless power transfer system for roadway-powered moving electric vehicles," *IEEE Transactions on Industrial Electronics*, vol. 61, no. 3, pp. 1179–1192, Mar. 2014.

[20] F. Farajizadeh, D. M. Vilathgamuwa, D. Jovanovic, P. Jayathurathnage, G. Ledwich, and U. Madawala, "Expandable N-legged Converter to Drive Closely Spaced Multitransmitter Wireless Power Transfer Systems for Dynamic Charging," *IEEE Transactions on Power Electronics*, vol. 35, no. 4, pp. 3794-3806, Apr. 2020.

[21] C. Hong, O. Shimizu, S. Nagai, T. Fujita, and H. Fujimoto, "Experimental Verification of N-phase Inverter Connected to Multiple Coils for Dynamic Wireless Power Transfer," *The 7th IEEJ international workshop on Sensing, Actuation, Motion Control, and Optimization*, Chiba, Japan, pp. 316-321, Mar. 2021.

[22] Y. Shanmugam, R. Narayanamoorthi, P. Vishnuram, D. Savio, A. Yadav, M. Bajaj, A. Nauman, T. Khurshaid, and S. Kamel, "Solar-powered five-leg inverter-driven quasi-dynamic charging for a slow-moving vehicle," *Frontiers in Energy Research*, vol. 11, Mar. 2023.

[23] K. Kusaka, R. Kusui, J. Itoh, D. Sato, T. Shijo, S. Obayashi, and M. Ishida, "A 22kW Three-phase Wireless Power Transfer System in Compliance with CISPR 11 and ICNIRP 2010", *IEEJ Journal of Industry Applications*, vol. 11, no. 4, pp. 594-602, Jul. 2022.

[24] O. Shimizu, T. Fujita, S. Nagai, H. Fujimoto, and Y. Omori, "Development of dynamic wireless power transfer coils for 3rd generation wireless in-wheel motor," *Electrical Engineering in Japan*, vol. 214, no. 4, Dec. 2021.